Waveguide Design Optimization for Compact Silicon Photonic Ferroelectric Phase Shifters

M. MISHRA,[1] N. R. DAS,[1,*] F. MORICHETTI[2]

[1]*Institute of Radio Physics and Electronics, 92, A.P.C. Road, University of Calcutta, Kolkata, 700009, India*
[2]*Dipartimento di Electtronica, Informazione e Bioingegneria, Politecnico di Milano, Via Ponzio 34/5, 20133, Milano, Italy*
**Corresponding author: nrd@ieee.org*

Received XX Month XXXX; revised XX Month, XXXX; accepted XX Month XXXX; posted XX Month XXXX (Doc. ID XXXXX); published XX Month XXXX

In this paper, a new design for ferroelectric BaTiO3 cladded silicon photonic phase shifter with very small switching length for compact Photonic Integrated Circuits (PICs) is proposed. The proposed design is based on the choice of a waveguide core with suitably slanted side walls in order to favour the desired polarization of ferroelectric cladding and to make guided modes spread towards the ferroelectric cladding with the consequence of further reduction in switching length compared to conventional (rectangular core) structure. The proposed design also gives additional benefit of having identical switching length for both TE and TM modes with the same configuration. These results offer a viable strategy to realize compact non-volatile phase shifters for reconfigurable and programmable PICs.

http://dx.doi.org/10.1364/AO.99.099999

Key words. Phase shifter, compact, ferroelectric, slanted side wall.

1. INTRODUCTION

In recent years, programmable PICs have drawn wide research interest for applications in many fields, like microwave photonics (MWP), classical and quantum information processing, machine learning etc. [1-3]. Like their electronic field-programmable gate arrays (FPGAs) counterpart, programmable PICs enable post fabrication manipulation and on-demand reconfiguration, with additional advantages in terms of speed, efficiency, immunity to EM interference etc. [4-6]. However, miniaturization of programmable PICs is essential for its useful implementation. Programmable PICs can be made of two dimensional photonic meshes of Mach-Zehnder (MZ) couplers arranged in square, triangular and hexagonal configurations [1, 3]. The unit cell area is responsible for footprint of the whole PIC, which is proportional to the length of the MZ couplers and of the phase shifters employed in between. So, reduction of the size of photonic phase shifters is essential to increase the integration density for use in reconfigurable and programmable PICs.

A phase shifter or a phase modulator is one of the most crucial components for programmable PICs. Several methods like, thermo-optic effect [7-12] and carrier injection/depletion effect in doped waveguides have been successfully used for realization of phase shifters [3, 13-17]. Phase shifters realized using such techniques, need continuous power supply for holding the changed phase of the light for a desirable period. Conventional thermo-optic effect based phase shifters are slow and additionally induce severe thermal crosstalk in densely integrated PICs. To overcome the limitations of above mentioned phase shifters, ferroelectric materials are currently being employed for the design of efficient photonic components [18-22]. The non-volatile nature of refractive index change of ferroelectric materials on application of electric field, helps the photonic components to be quite energy efficient, which is another important requirement for the PICs. $BaTiO_3$ (BTO) is an important ferroelectric material to serve this purpose. Being a uniaxial material, BTO changes its refractive index from ordinary axis n_o = 2.41 to extraordinary axis n_e = 2.36 by tracing the orientation of its domains from in-plane (a-axis) to out-of-plane (c-axis) on application of a suitable electric field (both in magnitude and orientation) [23]. This huge change in refractive index i.e. Δn = 0.05 is fast (occurs within few 10s of μs) and non-volatile (until more than one week), and hence providing a great opportunity for BTO to be used as cladding material to the waveguide core and helps in realization of fast, non-volatile and energy efficient optical phase shifters [24,25]. Fast domain switching nature of BaTiO3 has also been successfully utilized to develop high speed light modulators (40-65 GHz) [26-28]. A model for the analysis of ferroelectric switching in BTO cladded silicon waveguides has been reported by the authors in [29].

In the present study, the method described in [29] is employed to optimize the design of extremely compact non-volatile phase shifters integrated in silicon waveguides. In Section 2, the design rules followed for the minimization of the switching length are described with the support of an extensive numerical analysis. In Section 3, the switching behavior of the waveguide structure as a function of applied voltage is discussed in details. A concluding section summarizes the main achievements of this work.

2. WAVEGUIDE STRUCTURE

Section 2 is divided into two parts, the first one anticipating the main features of the of the proposed waveguide structure, the second one discussing the design rules followed to identify the optimized design.

A. Concept

The schematic of the proposed structure for a non-volatile phase shifter integrated in silicon waveguide is shown in Fig. 1. The phase shifter is a simple ridge waveguide structure, consisting of a Si core on SiO_2 substrate covered by BTO cladding on three sides and having three independent thin electrodes. Device parameters such as core width (w), cladding thickness (t) and electrode positions (core-side electrode gap (d_{el})) are varied over a practical range of values to obtain the optimum value for each of them. The direction of propagation of light is taken along x-axis, while the width and height of the waveguide are considered as y and z-axes respectively.

Since two values of the silicon core heights (220 nm and 300 nm) are conventionally employed in silicon photonics platforms, two waveguide designs are here optimized. We designate the waveguide with 220 nm of core height as structure S220, and that with 300 nm of core height as structure S300. According to the study reported in the next section, slanted sidewalls contribute to higher mode overlap with the BTO cladding and so to smaller switching length of the phase shifter. However, considering the feasibility of fabrication, the minimum slant angle is set to 70^0 throughout the study [30].

The native orientation of domains in the BTO cladding is assumed along a-axis (y-axis). To reduce the optical loss due to the electrodes, thin (100 nm) indium-tin-oxide (ITO) electrodes are considered. The basis of selection of other parameters are discussed in the next section.

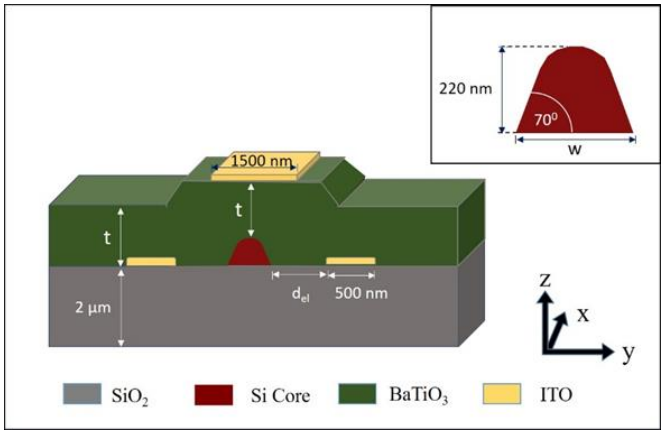

Fig. 1. Schematic of device structure. Inset shows zoomed view of Si core.

Throughout the present study the proposed device undergoes two different sets of biasing configurations named as "biasing-1" and "biasing-2". In case of biasing-1, the top electrode is taken as positive and both the bottom side electrodes are grounded. In case of biasing-2, the right bottom electrode is taken as positive and the left one as grounded, leaving the top electrode floating. Biasing-1 is used to change the refractive index of BTO cladding from n_o (polarization along y-axis) to n_e (polarization along z-axis) when a π phase shift in the propagating light is needed. Similarly, biasing-2 is used to take the BTO cladding to its initial refractive index value (from n_e to n_o) when no phase shift is required. These biasing arrangements are suitable for switching polarization by 90^0.

B. Design rules

The performance of the designed structure was studied through numerical simulations based on finite element method. Since the phase shifter is based on the electro-optic effect, it is important to get a favourable orientation of applied electric field within the cladding region to get the cladding refractive index changed from n_o to n_e. This could be done by tracing the local electric field of the cladding region as shown in our previous work [29]. However, close to the waveguide core (where the evanescent tail of the guided mode is stronger) the orientation of electric field is not optimum, thus lowering the electro-optic efficiency and resulting in an increase of the switching length of the phase shifter [29]. To obtain the desired orientation of electric field around the core, the structure parameters are tailored to favour the polarization of the ferroelectric domains and hence the reduction of switching length of the phase shifter. The choice of core shape, core width (w), cladding thickness (t) and core-side electrode gap (d_{el}) is described in the following subsections.

1. Shape optimization of the waveguide core

Figure 2 shows a comparative study for the mode distributions and switching length of the phase shifter for π phase shift with respect to different cladding thickness for the structure S220 (with a width w = 300 nm and t = 1200 nm) and ~~the corresponding~~ its conventional (rectangular core) structure without slanting the side walls.

As it can be seen from Fig 2(a), the shape of both TE and TM modes are more prominently pushed upwards to the ferroelectric BTO cladding in the proposed structure than in the conventional rectangular structure shown in Fig 2(b). This gives rise to a phase shifter with smaller length ~~and low operating voltage~~. Qualitatively, the same behaviour holds for structure S300 also. The switching lengths for both structures (with their corresponding rectangular counterparts) are shown in Fig 2 (c) and (d) respectively ~~for an applied voltage of 30V~~. The detailed study of the voltage required to achieve the desired switching length is given in Sec. 3. Results show that the slanted waveguide shape provides better performance for both core heights than the rectangular core shape. The main benefit in terms of switching length reduction is observed in waveguide S300, where TE and TM modes are both tightly confined in the waveguide core when the waveguide core is rectangular, but they both increase the mode overlap with the BTO cladding when the sidewalls are slanted. In the waveguide S220, where the TE and TM modes have a much different overlap with the upper cladding when the waveguide core is rectangular, slanting the sidewalls makes the switching length become almost polarization independent for a BTO thickness higher than 400 nm.

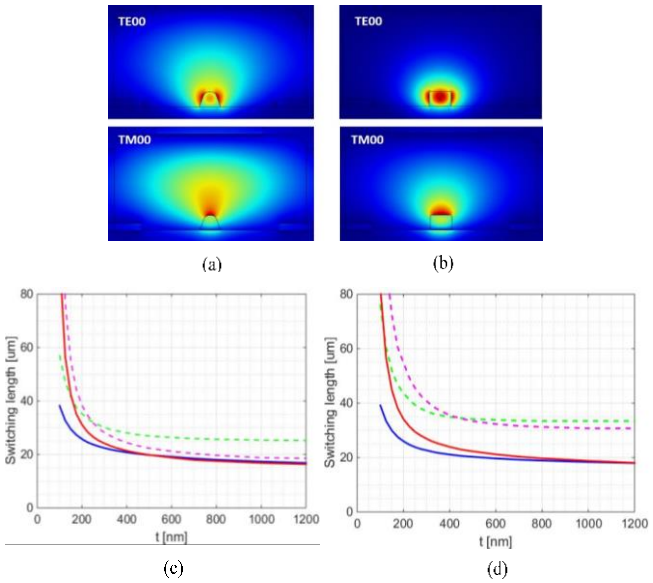

Fig. 2. (a) Mode distributions for waveguide S220 and (b) corresponding rectangular core structure, (c) Switching length vs cladding thickness (t) for both TE mode (blue line) and TM mode (Red line) for S220 and (d) S300, with corresponding rectangular structures (TE-green dashed line and TM-magenta dashed line). The width of WG is 300 nm for both the cases.

Besides increasing the overlap of the guided mode with the upper cladding material, an additional benefit of a waveguide core with slanted sidewalls is shown in Fig. 3. This figure shows a comparative plot of the electric field distribution around the core of S220 (with w = 300 nm and d_{el} =800 nm) and its corresponding rectangular core structure when a voltage of 1 V is applied between the electrodes for both biasing configurations. Figures 3(a) and (b) show the field orientation in the conventional structure and the proposed structure (S220) respectively for biasing-1. As mentioned earlier, this case of biasing is aimed to get the domains of ferroelectric BTO cladding oriented along z-axis (vertical direction) to change the refractive index of cladding from n_o to n_e. However, a close look towards the rectangular core structure in Fig. 3(a) shows that, local electric field orientation in the cladding region close to the core top is mainly along y-axis (red circled). This forces the domains of respective area remain oriented along y-axis and, hence, the refractive index of that particular area remains unchanged [29]. This leads to no phase change of light in that region. On the other hand, that particular area plays a crucial role in phase modulation of light, as the evanescent mode has more presence there (see Fig. 2(b)). This leads to requirement of long length for π phase shift to occur.

This problem can be solved by tilting the sidewalls and smoothing the waveguide top according to a curved shape as shown in Fig. 3(b). Figures 3(c) and (d) show field orientation for the same waveguide structures for biasing-2. In this case, the ferroelectric domains of the BTO cladding are aimed to get oriented along y-axis (horizontal direction) to retrieve the change of refractive index in ferroelectric cladding. However, the rectangular core structure (Fig. 3(c)) shows that local electric field orientation in the cladding regions adjacent to both side walls of the core are mainly along z-axis (red circled regions). As a result, the domains of these regions remain oriented along z-axis and accordingly refractive index there remains unchanged. This effectively increases the switching length of the phase shifter, since the amplitude of evanescent mode is more in these regions. But, looking towards the field orientation in the proposed structure in Fig. 3(d), it can be seen that, this field orientation problem is resolved to a great extent because of its curved top surface and tilted side walls. This helps the phase modulation to occur in a much shorter length. This feature is inherently related to the tilted profile of the proposed waveguide geometry and cannot be achieved by simply narrowing the core of a rectangular waveguide, which would only provide an increase of the mode overlap with the upper cladding.

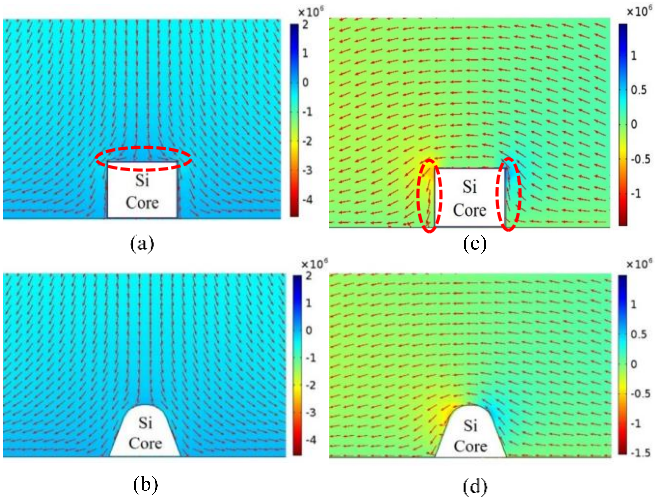

Fig. 3. Electric field orientation in the cladding adjacent to the core for biasing-1 in (a) rectangular, and (b) proposed core shape, and for biasing-2, in (c) rectangular, and (d) proposed core shape. The magnitude of the field (colored background) correspond to biasing of 1V in both the cases. Since the electric field orientation does not change with the applied voltage, these profiles apply also to higher voltages considered in the following of the paper .)

The choice of core width is important to reduce the switching length for both TE and TM modes. Figure Fig. 4(a) and (b) show that the switching length reduces as the core width is lowered. This result is expected because of the lower confinement of the guided modes in narrower waveguides. Interestingly, at a width w = 300 nm the switching lengths for TE and TM modes are identical for both structures provided that the BTO cladding is sufficiently thick. This is because, in the proposed design the evanescent tail of the TE and TM modes exhibit the same overlap with the BTO cladding unlike the conventional (rectangular) core shape. More in detail, for a 220 nm silicon core waveguide the meeting point comes at a thinner BTO layer (t = ~ 500 nm in Fig. 4 (a)), whereas for a 300 nm silicon core a thicker BTO layer is required (t = ~ 900 nm in Fig. 4 (b)). In wider waveguides, for instance when w = 400 and 500 nm, the cross over of the two modes requires a lower BTO thickness but occurs at a higher switching length . All these considerations make 300 nm as the preferred width for the proposed design. It should be noted that for this waveguide width the switching length for both structures is very similar. Figure 4(a) also shows that for the 220 nm thick waveguide the TM switching length is almost independent of the waveguide width because the mode confinement does not change significantly (see also inset of Fig. 5).

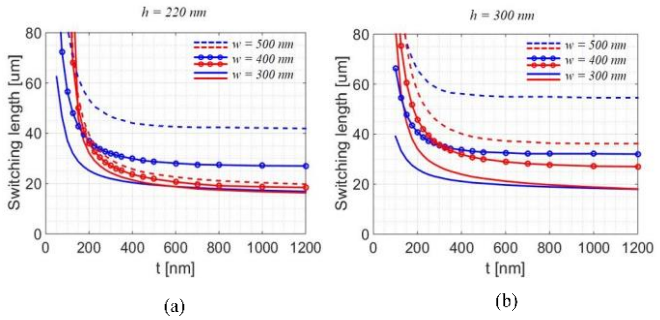

Fig. 4. Figure shows the required switching length (for π phase shift) for TE (blue) and TM (red) fundamental modes as a function of cladding thickness for (a) 220 nm and (b) 300 nm core heights and three different values of core widths for 70° bending of core side walls. The solid line, circled line and dashed lines represent results for w=300 nm, 400 nm and 500 nm respectively

1. Electrode Loss

The optimization of the BTO cladding thickness (t) and spacing (d_{el}) between core sidewall and bottom electrodes requires also considerations on the excess insertion loss induced by the electrode absorption. To keep loss negligible, a minimum value of d_{el} and t should be used. On the other hand, a larger electrode spacing implies a higher voltage for obtaining the desired switching effect. Table-1 reports the loss induced by the ITO electrodes when the waveguide width is 300 nm and the phase shifter has a length equal to the optimized switching length (see Fig. 4), that is 16 µm for waveguide S220 and 18 µm for S300. Results show that, in order to have about 0.1 dB loss for TE polarization, t > 1000 nm and d_{el} about 800 nm should be used for S220 waveguide (5th row of the table). For waveguide S300, d_{el} can be reduced to about 600 nm (2nd row of the table). As the electrode spacing (between side electrodes) is changed, the width of the top electrode should also be changed in a way to maintain the same orientation of the field between top electrode and ground electrodes. It is seen for this case that, for d_{el} = 800 nm it is taken as 1500 nm, and for d_{el} = 600 nm, it is taken as 1100 nm.

The structure has been finalized based on the above discussions with the optimum values of the parameters and the parameters are summarized in Table 2. The performance of the optimized structures based on the variation of switching length with core width is shown in Fig. 5. In this analysis, we limited the narrowest core width to 300 nm, because below this size fabrication issue arise [1] as well as an increase of scattering loss and backscattering phenomena is observed [2]. Figure shows the switching length achieved for S220 and S300 as 16 µm and 18 µm respectively for both TE and TM modes. This can be explained based on the mode-cladding overlapping as shown in inset of Fig. 5. The overlapping increases with decrease in core width for both the structures. It is also more for short height core. These two effects together result in achieving the highest mode-cladding overlapping for the given structure (S220).

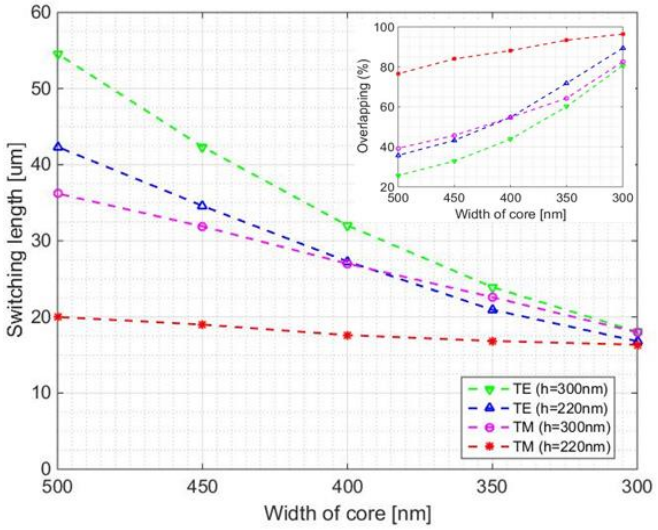

Fig. 5. Required switching length of both TE and TM modes for both core heights with fixed core shape as a function of core width in a decreasing order. Inset shows the mode-cladding overlapping as a function of core width. with tables and equations, figures should be set as one column wide

Table 1. Excess loss induced by the ITO electrodes for TE and TM modes for both S220 and S300 as a function of cladding thickness and side electrode spacing.

Sl. No.	t (Cladding Thickness) (nm)	d_{el} (Core-Side electrode gap) (nm)	Loss in dB (h=220 nm) L=16 µm		Loss in dB (h=300 nm) L=18 µm	
			TE	TM	TE	TM
1	1000	500	0.2362	1.2306	0.1775	0.4920
2	**1000**	**600**	0.1781	1.0741	**0.1175**	**0.3918**
3	1000	700	0.1434	0.9693	0.0852	0.3352
4	1000	800	0.1217	0.8978	0.0669	0.3020
5	**1200**	**800**	**0.1010**	**0.6548**	0.0556	0.2110

Table 2. Design values of S220 and S300 with w = 300 nm and slant angle = 70^0 for both the cases.

Parameters	Design Values of Structure-S220	Design Values of Structure-S300
Thickness of Cladding (t) in nm	1200	1000
Core to Side electrode Spacing (d_{el}) in nm	800	600
Top Electrode Width in nm	**1500**	**1100**
Minimum Switching Length (TE and TM) in µm	16	18

3. SIMULATION STUDY FOR BIAS DEPENDENCE OF SWITCHING LENGTH

In this section we study the dependence of the switching length of the proposed structure on the bias voltage by using the model reported in [29]. The electric field (normalized to the coercive field E_c) distribution across the waveguide cross section is plotted in Fig. 6. Fig. 6(a) shows the strength and orientation of the electric field for polarizing bias (biasing-1) used to switch the ferroelectric domains along the *z*-direction to change the refractive index of BTO cladding from n_o to n_e. It may be seen that, the local electric field components adjacent to the core have prominent *z* component along with magnitude that is higher than the coercive field, even at an applied voltage of 20 V. Fig. 6(b) shows the field orientation and magnitude for biasing-2 to get the polarization along *y*-direction, hence changing the refractive index of BTO from n_e to n_o. Here the field orientation is mainly along *y*-axis, which favours the desired *y* polarization of the domains in the cladding. This helps the BTO cladding getting its polarization switched easily. In this case, the field strength is higher on top of the core than in case of biasing-1. This is the indication for the fact that, polarization switching will also initiate at adjacent to core top along with the adjacent area of side electrodes.

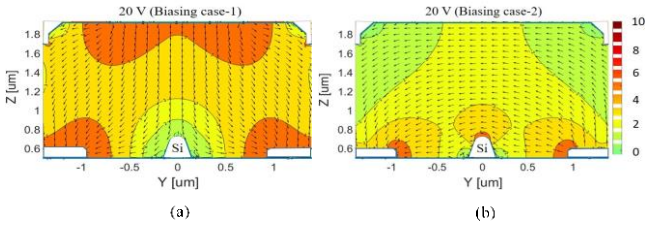

Fig. 6. Electric field magnitude (normalized to coercive field E_c = 25.2 kV/cm) with orientation for (a) biasing-1 and (b) biasing-2.

Figure 7 shows the plot for *z*-component of refractive index profile (n_z) for different applied voltages under both the biasing conditions. Figure 7(a) shows that the refractive index change occurs over a wide region of the cladding with voltage. When the applied electric field exceeds the coercive field (which is assumed to be E_c = 25.2 kV/cm) polarization switch (blue area) starts at the top of the BTO cladding and gradually becomes wider by covering the whole cladding upon application of an appropriate voltage. This changes the refractive index of cladding from n_o (red) to n_e (blue) and hence causes a phase shift in the light propagating through the phase shifter. Similarly, to get the phase shifter back to its initial polarization state, biasing-2 is applied, as shown in Fig. 7(b). The refractive index change (n_e to n_o) is nucleated (red area) mainly in the region adjacent to the core top after application of a suitable amount of voltage. A gradual increase in voltage, results in rapid increment of the red patch covering most of the BTO cladding except two small regions at the bottom corners. Similarly, the plot for y-component of refractive index profile (n_y) for different applied voltages under both the biasing conditions can be shown with indices values (2.41, 2.36) swapped. In both the cases of biasing, major part of the cladding region gets polarized for around 20 V and after 30V, there is no significant change in the plots, because all the domains have undergone a switch (saturation condition) and no significant change is observed.

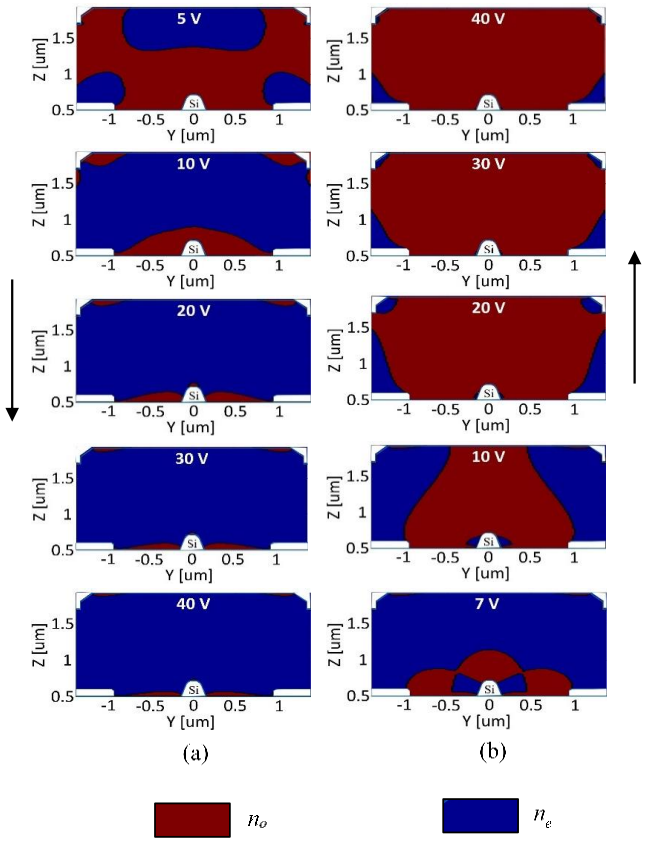

Fig. 7. Plot for refractive index (n_z) change of $BaTiO_3$ cladding with respect to different values of applied voltages for (a) biasing-1, and (b) biasing-2.

The plots for switching length (for π phase shift) versus applied bias for both biasing conditions are shown in Fig. 8. Figure 8(a) shows results for S220 with biasing-1. Up to 10 V of applied bias, the switching length reduces rapidly. Beyond 10 V, the reduction rate decreases and becomes extremely small after 20 V. In agreement with results shown in Fig. 4, the switching length for TE and TM modes are almost identical. Figure 8(b) shows the switching length for compensating the obtained π shift in the propagating light for S220 with biasing-2. In this case, since the polarization (refractive index) change initiates adjacent to the core, the switching length variation is sharp below 10 V and after that the variation is very small. The switching lengths for both the modes are similar to that obtained in case of biasing-1. It implies that, the initial polarization can be retrieved almost completely.

Similarly, Fig.8(c) and (d) shows the results for S300 for biasing-1 and biasing-2 respectively. In this case, the core has larger height and sharper top than that of S220 (since tilted angle is identical). Hence, the polarization (along *z*-axis) is expected to be more favourable in S300 than S220. In Fig. 8(c), the switching lengths for both the modes are same and unchanged after 20 V. Similar effects also take place for biasing-2 except the fact that, below 15 V, the switching lengths show a little mismatch. However, both the structures succeed to obtain the desired switching length within 30 V of applied bias.

Results in Figs. 7 and 8 suggest that it is not necessary that all the BTO domains of the waveguide cladding need to be switched in order to achieve the desired amount of phase shift. This means that the proposed device can be used also to introduced a continuous phase shift between 0 and π by suitably control the bias voltage from 5V to 20V.

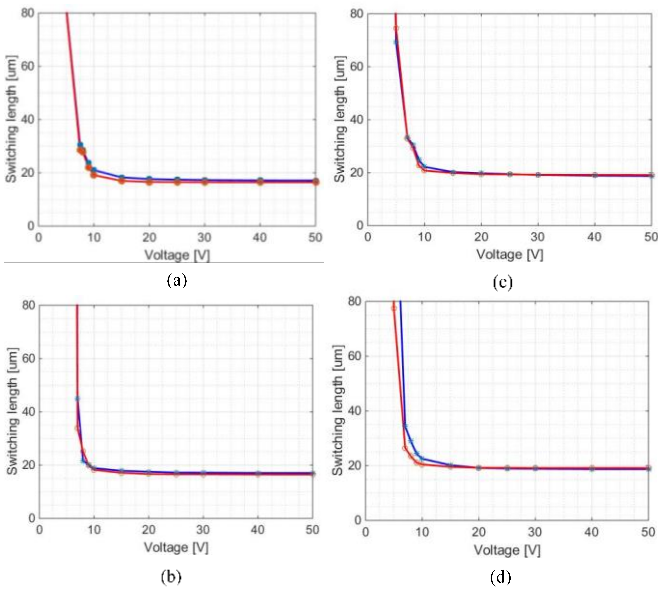

Fig. 8. Switching length vs. applied voltage for S220 with (a) biasing-1 and (b) biasing-2, and for S300 with (c) biasing-1 and (d) biasing-2.

4. CONCLUSION

A new design has been proposed for the realization of compact non-volatile phase shifter integrated in silicon waveguides which exploit domain switching in ferroelectric cladding material. The proposed device has a core shape with slanted sidewalls that increases the mode overlap with the BTO cladding and favours the desired polarization adjacent to the core. A systematic numerical investigation has been carried out to identify design rules for the waveguide core and the electrode configurations in order to achieve the best performance. As a result, a significant increases of the phase shift along the phase shifter is demonstrated, resulting in a >40% reduction of the switching length (e.g. 16 µm for S220 and 18 µm for S300 structures) compared to their respective conventional rectangular structures.

The proposed waveguide design can also be used in other type of phase shifter, modulators, sensors, and other photonic devices, where the overlap of the evanescent tail of the guided mode with the cladding material needs to be maximized. With such type of advantages, the proposed design can lead PIC technology far forward in the direction of energy efficiency and miniaturization.

Funding Information. M. Mishra acknowledges the financial support under the INSPIRE Fellowship program [IF150280] of Department of Science and Technology (DST), Govt. of India.

Acknowledgment. The authors wish to acknowledge Prof. Andrea Melloni of Politecnico di Milano, Milan, Italy, for his useful advice in this collaborative research work which was initiated through Erasmus Mundus LEADERS program (2014-2018).

References

1. N. C. Harris, J. Carolan, D. Bunandar, M. Prabhu, M. Hochberg, T. Baehr-Jones, M. L. Fanto, A. M. Smith, C. C. Tison, P. M. Alsing, and D. Englund, "Linear programmable nanophotonic processors," Optica 5, 1623 (2018).
2. D. Perez, Ivana Gasulla "Toward Programmable Microwave Photonics Processors," Journal of light wave technology 36, 519 (2018).
3. J. Carolan, C. Harrold, C. Sparrow, E. Martin-Lopez, N. J. Russell, J. W. Silverstone, P. J. Shadbolt, N. Matsuda, M. Oguma, M. Itoh, G. D. Marshall, M. G. Thompson, J. C. F. Matthews, T. Hashimoto, J. L. O'Brien, and A. Laing, "Universal linear optics," Science 349, 711 (2015).
4. L. Zhuang, C. G. H. Roeloffzen, M. Hoekman, K. Boller, and A. J. Lowery, "Programmable photonic signal processor chip for radiofrequency applications," Optica 2, 10(1–6) (2015).
5. J. Capmany, I. Gasulla, and D. P´erez, "Microwave photonics: The programmable processor," Nature Photonics 10, 1(6–8) (2016).
6. Daniel Pérez, Ivana Gasulla,1 José Capmany, and Richard A. Soref, "Reconfigurable lattice mesh designs for programmable photonic processors", Optics Express 24, 12093 (2016).
7. Xin Tu, C. Song, T. Huang, Z. Chen and H. Fu, "State of the Art and Perspectives on Silicon Photonic Switches", Micromachines 10, 51; doi:10.3390/mi10010051 (2019).
8. M. W. Pruessner, T. H. Stievater, M. S. Ferraro, and W. S. Rabinovich, "Thermo-optic tuning and switching in SOI waveguide Fabry-Perot microcavities", Optics Express 15, 7557 (2007).
9. J. Song, Q. Fang, S. H. Tao, T. Y. Liow, M. B. Yu, G. Q. Lo, and D. L. Kwong , "Fast and low power Michelson interferometer thermo-optical switch on SOI", Optical Society of America 15, 15304 (2008).
10. I. Kiyat, A. Aydinli and N. Dagli, "Low-Power Thermooptical Tuning of SOI Resonator Switch", IEEE Photonics Technology Letters 18, 364 (2006).
11. A. Densmore, S. Janz, R. Ma, J. H. Schmid, D.-X. Xu, A. Delâge, J. Lapointe, M. Vachon, and P. Cheben,"Compact and low power thermo-optic switch using folded silicon waveguides", Optical Society of America 17, 10457 (2009).
12. Y. Li, J. Yu, and S. Chen "Rearrangeable nonblocking SOI waveguide thermooptic 4×4 switch matrix with low insertion loss and fast response", IEEE Photonics Technology Letters 17, 1641 (2005).
13. Q. Xu, S. Manipatruni, B. Schmidt, J. Shakya, and M. Lipson "12.5 Gbit/s carrier-injection-based silicon microring silicon modulators", Optics Express 15, 430 (2007).
14. C. Li, L. Zhou, and A. W. Poon, "Silicon microring carrier-injection-based modulators/switches with tunable extinction ratios and OR-logic switching by using waveguide cross-coupling", Optics Express 15, 5069 (2007).
15. J.-B. You, M. Park, J.-W. Park, and G. Kim, "12.5 Gbps optical modulation of silicon racetrack resonator based on carrier-depletion in asymmetric p-n diode", Optics Express 16, 18340 (2008).
16. N.-N. Feng, S. Liao, D. Feng, P. Dong, D. Zheng, H. Liang, R. Shafiiha, G. Li, J. E. Cunningham, A. V. Krishnamoorthy, and M. Asghari, "High speed carrier-depletion modulators with 1.4V-cm VπL integrated on 0.25µm silicon-oninsulator waveguides", Optics Express 18, 7994 (2010).
17. Z. -Y. Li, D. -X. Xu, W. R. McKinnon, S. Janz, J. H. Schmid, P. Cheben, and J. -Z. Yu, "Silicon waveguide modulator based on carrier depletion in periodically interleaved PN junctions", Optics Express 17, 15947 (2009).
18. S. Abel, T. Stö ferle, C. Marchiori, D. Caimi, L. Czornomaz, M. Stuckelberger, M. Sousa, B. J. Offrein, and J. Fompeyrine, "A Hybrid Barium Titanate–Silicon Photonics Platform for Ultraefficient Electro-Optic Tuning", Journal Of Lightwave Technology 34, 1688 (2016).
19. S. Abel, T. Stöferle, C. Marchiori, D. Caimi, L. Czornomaz, C. Rossel, M. D. Rossell, R. Erni, M. Sousa, H. Siegwart, J. Hofrichter, M. Stuckelberger, A. Chelnokov, B. J. Offrein, and J. Fompeyrine, "Electro-Optical Active Barium Titanate Thin Films in Silicon Photonics Devices", Advanced Photonics Congress (OSA), 2013. (https://doi.org/10.1364/IPRSN.2013.IW4A.5)
20. C. Xiong, W. H. P. Pernice, J. H. Ngai, J. W. Reiner, D. Kumah, F. J. Walker, C. H. Ahn, and H. X. Tang, "Active silicon integrated nanophotonics: ferroelectric BaTiO3 devices", NANO Letters 14, 1419 (2014).
21. K. Alexander, John P. George, J. Verbist, K. Neyts, B. Kuyken, D. Thourhout and J. Beeckman, "Nanophotonic Pockels modulators on a silicon nitride platform", Nature Communication 9, 3444 (2018).
22. M. Hsu, A. Marinelli, C. Merckling, M. Pantouvaki, J. Campenhout, P. Absil & D. V. Thourhout, "Orientation dependent electro-optical response of BaTiO3 on SrTiO3-buffered Si(001) studied via Spectroscopic Ellipsometry", Optical Materials Express 7, 2030 (2017).

23. M. J. Dicken, L. A. Sweatlock, D. Pacifici, H. J. Lezec, K. Bhattcharya and H. A. Atwater, “Electrooptic Modulation in Thin Film Barium Titanate Plasmonic Interferometers”, Nano Letters 8, 4048 (2008).
24. I. M. Albo, S. Varotto, M. Asa, C. Rinaldi, M. Cantoni, R. Bertacco, and F. Morichetti, “Non-Volatile Switching of Polycrystalline Barium Titanate Films Integrated in Silicon Photonic Waveguides,” Advanced Photonics 2018 (BGPP, IPR, NP, NOMA, Sensors, Networks, SPPCom, SOF), OSA Technical Digest (online), paper ITu4I.2 ,Optical Society of America, (2018).
25. I. M. Albo, S. Varotto, M. Asa, C. Rinaldi, M. Cantoni, R. Bertacco, and F. Morichetti, “Integration of Non-Volatile Ferroelectric Actuators in Silicon Photonics Circuits,” 2018 20th International Conference on Transparent Optical Networks (ICTON), Bucharest, 2018, pp. 1-4.
26. Stefan Abel, Felix Eltes, J. Elliott Ortmann, Andreas Messner, Pau Castera, Tino Wagner, Darius Urbonas, Alvaro Rosa, Ana M. Gutierrez, Domenico Tulli, Ping Ma, Benedikt Baeuerle, Arne Josten, Wolfgang Heni, Daniele Caimi, Lukas Czornomaz, Alexander A. Demkov, Juerg Leuthold, Pablo Sanchis and Jean Fompeyrine “Large Pockels effect in micro- and nanostructured barium titanate integrated on silicon”, nature materials 18, 42 (2019).
27. Kristy J. Kormondy, Youri Popoff, Marilyne Sousa, Felix Eltes, Daniele Caimi, Marta D. Rossell, Manfred Fiebig, Patrik Hoffmann, Chiara Marchiori, Michael Reinke, Morgan Trassin, Alexander A. Demkov1, Jean Fompeyrine and Stefan Abel “Microstructure and ferroelectricity of BaTiO3 thin films on Si for integrated photonics”, Nanotechnology 28, 112436 (2017).
28. P. Tang, A.L. Meier, D.J. Towner and B.W. Wessels, “High-speed travelling-wave BaTiO3 thin-film electro-optic modulators”, ELECTRONICS LETTERS 41, 1296 (2005).
29. M. Mishra, N. R. Das, A. Melloni and F. Morichetti, “Modelling domain switching of ferroelectric BaTiO3 integrated in silicon photonic waveguides”, Optics Communications 448, 19 (2019).
30. Valerian Hongjie Chen, Jun Rong Ong & Ching Eng Png, “Polarisation independent silicon-on-insulator slot waveguides”, SCIENTIFIC REPORTS 6, 37760(1) (2016).